



# A PMIP3 narrative of modulation of ENSO teleconnections to the Indian summer monsoon by background changes in the Last Millennium

Charan Teja Tejavath<sup>1</sup> · Karumuri Ashok<sup>1</sup> · Supriyo Chakraborty<sup>2</sup> · Rengaswamy Ramesh<sup>3</sup>

Received: 29 June 2018 / Accepted: 6 March 2019 / Published online: 16 March 2019  
© Springer-Verlag GmbH Germany, part of Springer Nature 2019

## Abstract

Using nine model simulations from the PMIP3, we study simulated mean Indian summer (June–September) climate and its variability during the Last Millennium (LM; CE0850–1849) with emphasis on the Medieval Warm Period (MWP; CE1000–1199) and Little Ice Age (LIA; CE1550–1749), after validation of the simulated ‘current day (CE1850–2005)’ climate and trends. We find that the simulated above (below) mean-LM summer temperatures during the MWP (LIA) are associated with relatively higher (lower) moisture, and relatively higher (lower) number of concurrent El Niños (La Niñas). Importantly, the models simulate higher (lower) Indian summer monsoon rainfall (ISMR) during the MWP (LIA) compared to the LM-mean, notwithstanding a strong simulated negative correlation between NINO3.4 index and the area-averaged ISMR. Interestingly, the percentage of the simulated strong El Niños (La Niñas) associated with negative (positive) ISMR anomalies is higher (lower) in the LIA (MWP). This nonlinearity is explained by the simulated background climate changes, as follows. Distribution of simulated anomalous 850 hPa boreal summer velocity potential during MWP in models indicates, relative to the mean LM conditions, a zone of anomalous convergence in the central tropical Pacific flanked by two zones of divergence, i.e. a westward shift in the Walker circulation. The anomalous divergence centre in the west during the MWP also extends into the equatorial eastern Indian Ocean, triggering in an anomalous convergence zone over India and relatively higher moisture transport therein and therefore excess rainfall during the MWP as compared to the LM-mean, and hence an apparent weakening in the El Niño impact.

## 1 Introduction

Instrumental records of climate seldom date back prior to the 1850s. Therefore, analysis of proxy climate data, aided by climate modelling, has been the principal means to evaluate past climate variability. Past climate records exhibit

significant variability on millennial to interannual timescales (Stockett et al. 2013, henceforth referred to as TS-IPCC13). Interestingly, reports based on a large number of publications point out to significant centennial climate variations during the last two millennia (PAGES 2 k Consortium, 2013; TS-IPCC13). Paleo-data based studies identify two significant periods in the last millennium (LM), i.e. Common Era (CE) 0850–1849, prior to when the instrumental observations started. These two periods are, (1) a relatively warmer period known in literature as the ‘Medieval Warm Period’ (MWP, CE 950–1350), roughly followed by (2) a relatively cooler period, the Little Ice Age (LIA, CE 1500–1850) (e.g. Lamb 1965; Grove 1988; Graham et al. 2010; Mann et al. 2009). The extent of these warmer (MWP) and cooler (LIA) periods varies from region to region in terms of timing, duration and magnitude of the temperature anomalies (Stocker et al. 2013; Dixit and Tandon 2016). Paleoclimate reconstructions from various well-dated proxy data suggest that during the MWP, some regions experienced temperatures as warm as mid-twentieth century, whereas some others such

---

Rengaswamy Ramesh: passed away on 2 April 2018.

---

**Electronic supplementary material** The online version of this article (<https://doi.org/10.1007/s00382-019-04718-z>) contains supplementary material, which is available to authorized users.

---

✉ Karumuri Ashok  
ashokkarumuri@uohyd.ac.in

<sup>1</sup> Centre for Earth, Ocean and Atmospheric Sciences, University of Hyderabad, Hyderabad, India

<sup>2</sup> Indian Institute of Tropical Meteorology, Pune, India

<sup>3</sup> School of Earth and Planetary Sciences, NISER, Bhubaneswar, India

as the extratropics, southern hemisphere land region were as warm as the late-twentieth century (TS-IPCC13). As can be seen, these studies do not report the conditions at a regional scale. Particularly, there are no proxy or modelling studies that have reported on the temperature conditions over the Indian subcontinent, which is a major hotspot of climate variability, largely from the perspective of the summer monsoon rainfall. The Indian Summer Monsoon Rainfall (ISMR; June–September; JJAS) variability is manifested on intra-annual, interannual, decadal, centennial and millennial to multi-millennial time scales (Ramesh et al. 2010; Chakraborty et al. 2012). Paleo-monsoon records from well-dated proxy data from the Arabian Sea (e.g. Sarkar et al. 2000; Gupta et al. 2003; Staubwasser et al. 2003; Tiwari et al. 2005), the Arabian Peninsula (e.g. Fleitmann et al. 2003, 2007; Neff et al. 2001), and the Indian subcontinent (e.g. Berkelhammer et al. 2012; Dixit et al. 2014a, b, 2015; Dixit 2013; Dutt et al. 2015; Nakamura et al. 2015) show centennial-to millennial-scale changes in the ISMR during the Holocene.

In a recent review, Dixit and Tandon (2016) suggest that MWP and LIA effects are well reflected in the ISMR, with a caveat that proxy data exhibit heterogeneity in terms of the timing and duration. Proxy records also suggest that during the last millennium, ISMR was the higher during the MWP and relatively weaker during the LIA (Yadava et al. 2005). However, the data density is rather sparse in time and space to quantify the decadal through the centennial scale temporal structure of ISMR variability during MWP and LIA.

A speleothem-based reconstruction of ISMR variability by Sinha et al. (2007) exhibits an evolution conforming to solar activity (for which atmospheric radiocarbon activity is used as a surrogate) only during the MWP. An increased summer monsoon precipitation during the MWP is suggested to be linked to the ENSO that has been modulated by solar forcing variations in a few proxy-data studies (Berkelhammer et al. 2010; Emile-Geay et al. 2007). The speleothem-based monsoon reconstruction of Sinha et al. (2007, 2011) suggests a severe weakening of Indian Summer Monsoon (ISM) during the LIA, apparently associated with multi-year to decades-long droughts particularly between thirteenth and seventeenth centuries. Another proxy record, from the Dandak cave in Central India, shows a 30% rainfall reduction during the fourteenth century (Yadava et al. 2005).

Obviously, the recent ~ 150-year period is the best documented period in terms of instrumental observations. Uncertainties, however, exist in terms of the quality and spatial density of data even for this period. The observational records of ISMR from the beginning of the last century show that its interannual and inter-decadal variability is significantly associated with that of the El Niño–Southern Oscillation (ENSO; e.g. Sikka 1980; Keshavamurthy 1982; see Ashok et al. 2004 for further references).

Typically, the warmer (cooler) ENSO events are associated with lesser (higher) than normal rain over India during the boreal summer, concurrent with the Indian monsoon season. Prasad et al. (2014), based on proxy climate data, infer that the long-term influence of ENSO like conditions on ISM began only 2ky BP, and is coincident with Southern Indo-Pacific warm pool (IPWP) warming. They also suggest that the IPWP-ISM links and large scale advection of moist air toward India vary on a multi-centennial scale. Kitoh et al. (2007), in a model study, observe decadal variability in the ENSO-ISM relation. Through a 31-yr moving correlation analysis, they show that, during the LM, the ISMR-ENSO correlations vary over a wide range, specifically  $-0.71$  to  $+0.07$ , with an overall correlation of  $-0.34$  for the LM.

Thus, the variability of Indian summer monsoon during the LM has been relatively less studied, particularly from the modelling perspective. It is also noticeable that all the model studies cited above (Kitoh et al. 2007; Prasad et al. 2014) primarily employed single GCMs. From this perspective, it is interesting to explore multi-model simulations such as those from the PMIP3, to study Indian summer monsoon conditions during the LM, specifically the MWP and the LIA. Such a study would obviously explore the capability of these models in capturing at least a millennium of the past climate. Importantly, it would also facilitate a quantification of the multi-model spread, which, if acceptably low, will provide a view of the climate of the relevant period that would complement the knowledge from proxy-data studies. Furthermore, such a multi-model study would serve as a benchmark for addressing longer periods of climate variability relevant to the Indian summer monsoon using models.

With this motivation, here we study the multi-model simulated ISMR variability and its teleconnections with the ENSO during the LM, using various relevant PMIP3 datasets with an emphasis on the simulated Medieval Warm Period (MWP; CE 1000–1199 as against the CE 0950–1350 from the proxy-observations) and Little Ice Age (LIA; CE 1550–1749 as against the CE 1500–1850 from proxy observations). To be clear, we consider the 200 warmest (relatively coldest) year-period as the simulated MWP (LIA) period for maintaining uniformity between global and regional analysis of ENSO-ISM teleconnections from the PMIP3 LM simulations, with the knowledge that the temporal and spatial signatures of the MWP and LIA varied from region to region, at least in terms of magnitude (e.g. Stocker et al. 2013; Dixit and Tandon 2016).

In the following section, we describe the various reanalysed, observed, and PMIP3 datasets we use. We present our results in the subsequent section, and provide a concluding summary in the last section.

## 2 Data and methodology

It is indeed a challenging prospect to validate the simulated Indian summer monsoon features from the PMIP3 simulations for the LM period, given the sparse and scanty observations. Fortunately, the corresponding model simulations of the CMIP5 vintage for the historical period (CE 1850–2005), i.e. the current day climate, can be validated using various observed/reanalysed gridded datasets, keeping in mind the uncertainties associated with such datasets during the pre-satellite period. Therefore, in this study, we start by exploring the fidelity of simulated Indian summer monsoon climate from historical simulations (henceforth referred to as HS) that cover the CE 1850–2005 period in which instrumental observations are available. Specifically, the criteria we adopt for validation of the historical model simulations are, the ability of the models to reproduce the observed trends in surface temperature and rainfall over India during the summer monsoon season, and to simulate the observed negative correlation between the ISMR and the concurrent NINO3.4 Index. It may be noted that this exercise is primarily carried out only for nine CMIP5 models for which the PMIP3 simulations for the LM period are available for the CE 0850–1849 period (LM), under the class termed as ‘past1000’ (henceforth referred to as p1000).

As outlined by Taylor et al. (2012), for the HS, the models were forced with observed atmospheric composition changes with natural and anthropogenic aerosols or their precursors, natural sources of short-lived species, and time-evolving land cover. On the other hand, the p1000 results were obtained by forcing the models with well-mixed greenhouse gases, changes in volcanic aerosols, land use, and solar irradiance changes (Taylor et al. 2012; Schmidt et al. 2011; Schmidt et al. 2012). The nine models whose simulation outputs were used in this study are: BCC-CSM1-1, IPSL-CM5A-LR, FGOALS-s2, MPI-ESM-P, GISS-E2-R, CCSM4, CSIRO-Mk3L-1-2, MRI-CGCM3 and HadCM3. These datasets have been downloaded from “<http://cera-www.dkrz.de/WDCC/ui/>

Index.jsp”. The acronyms used for the model simulations, are presented in Table 1. We evaluate the fidelity of the HS simulations by comparing with the observed Indian summer monsoon rainfall and various other reanalysed climate datasets. The various observational/reanalysed data sets used for the validation of the HS are, the Hadley Centre Interpolated sea surface temperature (HadISST; Titchner and Rayner 2014) for the CE 1870–2014 period, the ERA-20CM sea surface temperature (SST) and skin temperature (SKT) datasets (Hersbach et al. 2015) for the CE 1900 to 2010 period. (using two SST datasets throws light on any uncertainties associated with the data quality therein) and the India Meteorological Department (IMD) gridded rainfall datasets for CE 1901–2009 period (Rajeevan et al. 2006), available at 1.0° latitude × 1.0° longitude resolution and covering the land region bound by 66.5°E–101.5°E; 6.5°N–39.5°N. The Global Precipitation Climatology Project Version 2 (GPCP; Adler et al. 2003) and CPC Merged Analysis of Precipitation (CMAP; Xie et al. 1997) were used. The multi-level NCEP/NCAR Reanalysis version 1 datasets of horizontal winds available for the 1948–2009 period (Kalnay et al. 1996) are also used. For uniformity, all the simulated precipitation and near air surface temperature data sets were re-gridded to 2.0° latitude × 2.0° longitude resolution grids. The historical simulations from the individual models are validated by comparing various climate statistics with the corresponding climate statistics from observed and reanalysed datasets for the CE 1901–2005 period. As is the practice, the various reanalysis datasets are approximated to represent the ‘observations’.

We compute the well-known NINO3.4 index, which is defined as the area-averaged SST anomaly over the region bounded by 170°W–120°W; 5°S–5°N, to represent the ENSO variability. A representative Indian summer monsoon rainfall (ISMR) index, which we designate as the AAISMR, is obtained by area-averaging the mean June-through-September (JJAS) rainfall over the land region bounded by 65°E–95°E; 10°N–30°N. The area-averaged temperature for

**Table 1** CMIP5/PMIP3 Last Millennium and Historical simulations with their temporal span, and acronyms of the models used

S. no	CMIP5/PMIP3 models	p1000 (last millennium) simulation temporal coverage	Historical simulation temporal coverage	Acronyms
1	BCC-CSM1-1	CE 0850–1849	CE 1850–2005	BCC
2	CCSM4	CE 0850–1849	CE 1850–2005	CCSM4
3	IPSL-CM5A-LR	CE 0850–1849	CE 1850–2005	IPSL
4	MPI-ESM-P	CE 0850–1849	CE 1850–2005	MPI
5	GISS-E2-R	CE 0850–1849	CE 1850–2005	GISS
6	FGOALS-s2	CE 0850–1849	CE 1850–2005	FS2
7	HadCM3	CE 0850–1849	CE 1850–2005	HADCM3
8	CSIRO-Mk3L-1-2	CE 0850–1849	CE 1850–2005	CSIRO
9	MRI-CGCM3	CE 0850–1849	CE 1850–2005	MRI

the Indian region is also obtained by averaging the surface temperature over this region (AAISMT).

To check the ENSO-ISM relationship and its variability during LM, we calculate the monthly anomalies of surface temperature and precipitation from their respective climatological monthly means. The anomalies of any parameter, such as, say, the JJAS temperature, for each model have been obtained by subtracting the 1000-year climatological value of the individual seasonal values. Linear correlation analysis is used to estimate the ENSO-ISM relationship during various periods.

We carry out a trend analysis, the significance of which has been evaluated through the Mann–Kendall test. The statistical significance of linear correlation, and that of the partial correlation, has been evaluated using a 2-tailed Student's t-test. Further, while ascertaining the statistical significance of correlation differences from the MWP to LIA, we employ a bootstrapping test with 1000 simulations. We use the bootstrapping subroutine “bootstrap\_correl”, provided by the freely available NCL package from NCAR. This routine takes the two input time series (the model-simulated ISMR & NINO3.4 SSTA for MWP, for example, in our case) for which the correlations need to be obtained. Based on these input series, it generates 1000 timeseries pairs randomly, and computes correlations between each pair. After that, the correlations are ordered as per magnitude. The fifth highest correlation, for example, gives us the 0.005 significance level (i.e. 99.5% confidence level) for the correlations, and so on. In case of correlation differences between two simulations, such as the MWP & LIA simulations by the same model,

the differences of correlations are ordered as per magnitude to mark the significant threshold values.

### 3 Results

#### 3.1 Validation of the HS

Figure 1a, b respectively show the 11-year running mean of near-surface air temperatures averaged over the globe and that averaged over Indian region, from the nine models of the HS; Fig. 1c, d show the corresponding time series of anomalies. It is seen from Fig. 1c, d that all the models can simulate the observed increasing temperature trend reasonably, notwithstanding an inter-model spread. Further, we find that the observed as well as the simulated trends are significantly above the corresponding interannual standard deviations (Fig. 1). Figure 1d suggests that the surface temperatures over India have also continued to rise till the end of the twentieth century, which agrees with a study based on station observations (Revadekar et al. 2012). Several recent studies suggest a decreasing trend in Indian summer monsoon rainfall (e.g. Guhathakurtha et al. 2007; Krishnan et al. 2016; Sano et al. 2011) in recent decades. Figure 2a shows the observed and simulated AAISMR. The corresponding AAISMR anomalies are present in Fig. 2b. We find relatively higher inter-model spread in the AAISMR relative to the corresponding surface temperatures (Fig. 1b, d). We show the area-averaged climatological seasonal cycle of the Indian rainfall during CE 1901–2005 in Figure A1,

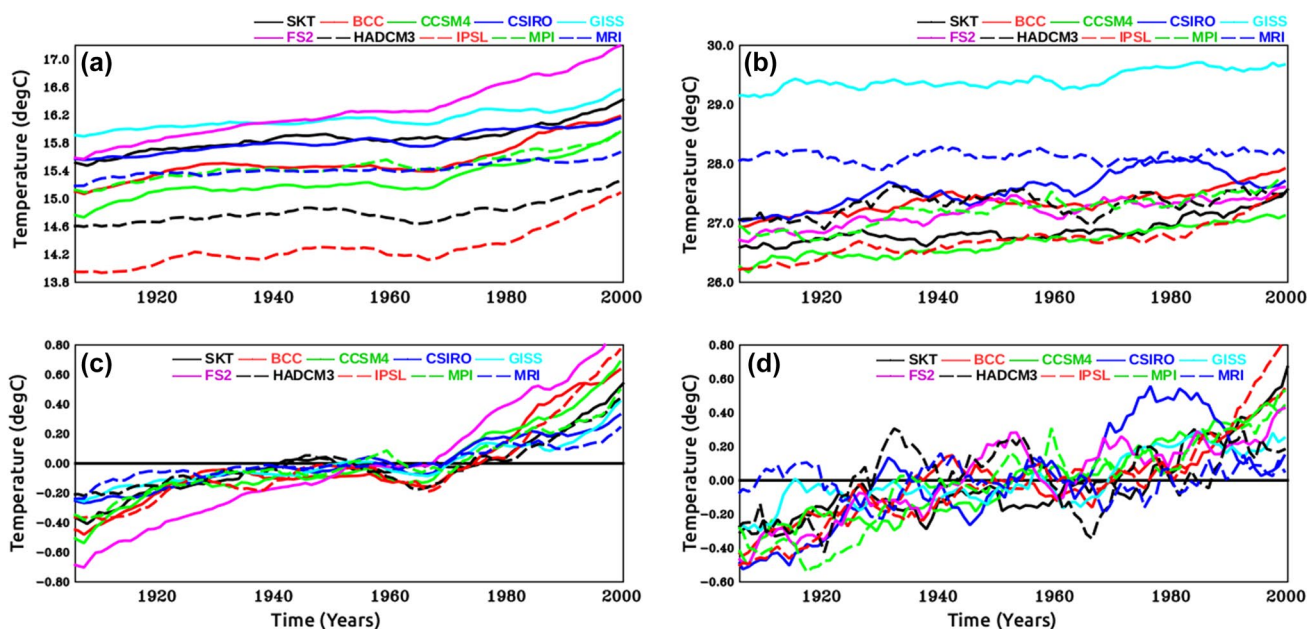


**Fig. 1** 11-year running mean of simulated surface air temperature ( $^{\circ}\text{C}$ ) obtained by area-averaging **a** globally **b** over India; the corresponding temperature anomalies ( $^{\circ}\text{C}$ ) are shown in panels **c** and **d**, respectively

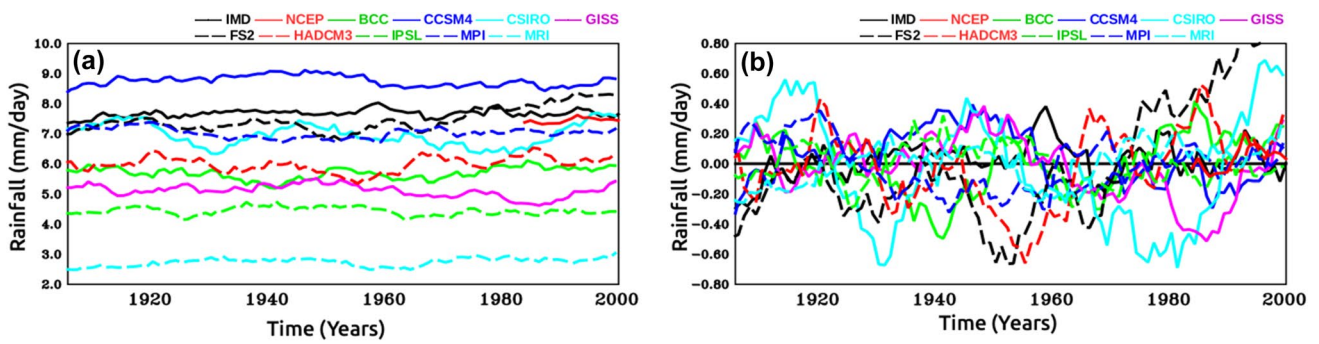


**Fig. 2** a 11-year running mean of simulated, and observed, area-averaged ISMR (mm/day) during the 1901–2005, and b corresponding anomalies (mm/day)

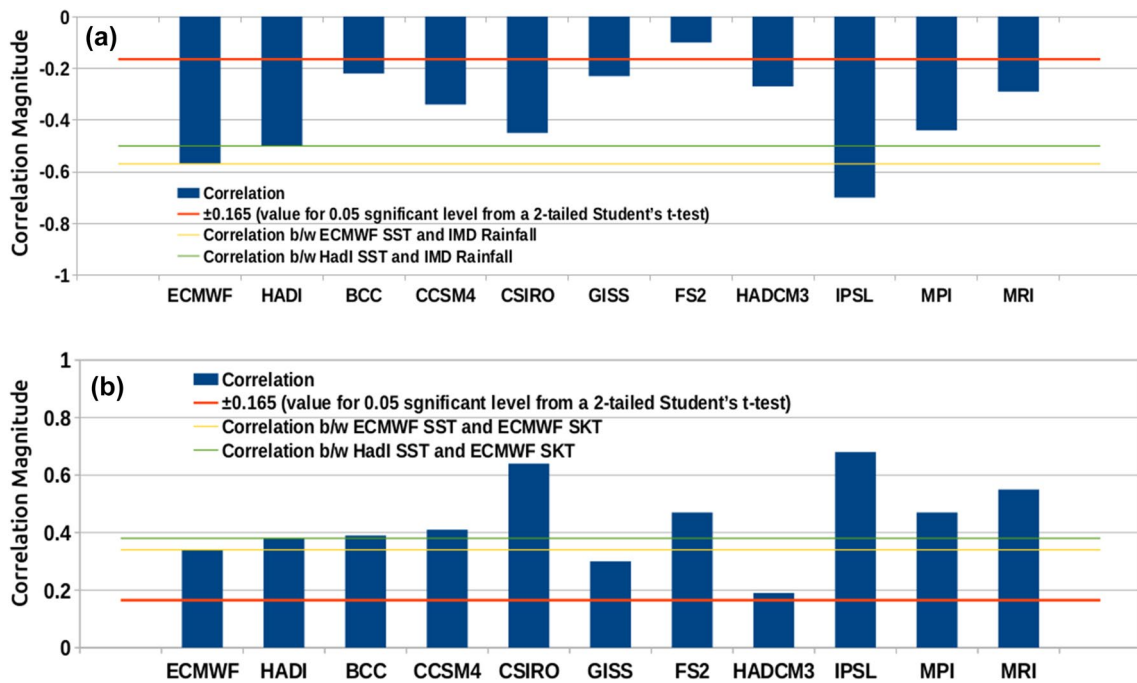


**Fig. 3** Correlations from historical data between the NINO3.4 and (a) AAISMR, (b) area-averaged near-surface air temperature over India of respective model simulations (red line represents the 0.05 significance level from a 2-tailed Student’s t-test, yellow and green lines represent the corresponding correlation values from observations)

and mean climatological distribution (CE 1979–2005) of the observed and model-simulated Indian summer monsoon rainfall in Figure A2. From Figures A1 and A2, it is evident that all the models except CCSM4 show a dry bias. We also find statistically significant decreasing trend at the end of the twentieth century in the AAISMR simulated by three models (CCSM4, GISS and MPI), in agreement with the observations. The trends in the other models are not statistically significant. The interannual standard deviation for these the area-averaged rainfall and temperature over India during JJAS, from observations as well as from the individual model simulations, are presented in Table A1. We

find that simulated standard deviations from various models fall within a  $\pm 20\%$  range of observations.

On a different note, an increase in warm ENSO events, be it canonical or Modoki (e.g. Ashok et al. 2007), has been observed in the late twentieth century with an increase in global temperature (e.g. Collin 2000; Cai et al. 2015). The models are able to reproduce this trend qualitatively to a reasonable extent, as seen by the higher number of simulated warm events, represented by the positive NINO3.4 index (Table A2).

That the ENSO is a major driver of interannual variability of the Indian summer climate is evidenced by

the negative correlation of  $-0.5$  (Fig. 3a) between the AAISMR and NINO3.4 index derived from the HadISST for the period CE 1901–2005, statistically significant at 0.01 level from a 2-tailed Student's t-test. Note that, the analogous correlation obtained by using the NINO3.4 index from the ECMWF SST data sets is  $-0.57$ . The corresponding NINO3.4-AAISMR correlations from the HS are also presented in Fig. 3a. Seven out of the nine models simulate the negative correlations with a range of  $-0.21$  to  $-0.51$ , which are statistically significant at the 0.05 significance level from a 2-tailed Student's t-test. The CCSM4 and FGOALS-s2 models simulate weaker correlation coefficients of  $-0.12$  (significant at 0.2 level) and  $-0.1$ , respectively.

The AAISMT (CE 1901–2005) yields moderate correlation coefficients of 0.34 and 0.38 with the concurrent NINO3.4 index from HadISST and that from the ECMWF SST datasets, respectively; both values are statistically significant at 0.05 level from a 2-tailed Student's t-test. Corresponding correlations of all the models are statistically significant at 0.05 level from a 2-tailed test, though they vary over a wide range of values varying from 0.19 to 0.74 (Fig. 3b).

In summary, the BCC-CSM1-1, IPSL-CM5A-LR, MPI-ESM-P, GISS-E2-R, CCSM4, HadCM3, CSIRO-Mk3L-1-2, MRI-CGCM3 and FGOALS-s2 models meet our criteria for their p1000 simulations to be used for further analysis to understand the LM variability.

### 3.2 p1000 analysis

To ascertain that there is a reasonable agreement of variability among the LM simulations from the models, we present in Table A3 the JJAS standard deviations ( $\sigma$ ) of the simulated area-averaged global surface temperatures, AAISMT, AAISMR and the NINO3.4 index for the whole period as well as three overlapping 500-year sub-periods, namely, CE 850–1349, CE 1100–1599, and CE 1350–1849. The simulated statistics from the individual models fall within the  $\pm 1\sigma$  range of the corresponding statistic (Table A3) in general, except the  $\sigma$  of the simulated NINO3.4 index from the FGOALS-s2 model. This shows that the simulated variabilities across the models are, in general, in reasonable agreement with one another.

Figure A3a shows a 101-year running average of a time series of globally-averaged simulated surface temperature for the JJAS season during LM i.e. from CE 0850–1849, (henceforth  $T_G$ ), and Figure A3b, the corresponding time series representing the surface temperature over the Indian subcontinent (henceforth  $T_I$ ). The 101-year running window has been applied to identify the long term changes. We note that the simulated signals in all the models evolve coherently in time, but with significant spread across the models.

To visualise the evolution more clearly, we calculate the 101-year running mean of temporal anomalies of the  $T_G$  (Fig. 4a) and  $T_I$  (Fig. 4b). We see a relatively more coherent inter-model evolution in the anomalies of the  $T_G$  (Figure A3a) as compared to the  $T_G$  (Figure A3b). Importantly, while there are fluctuations in temperature during LM, we

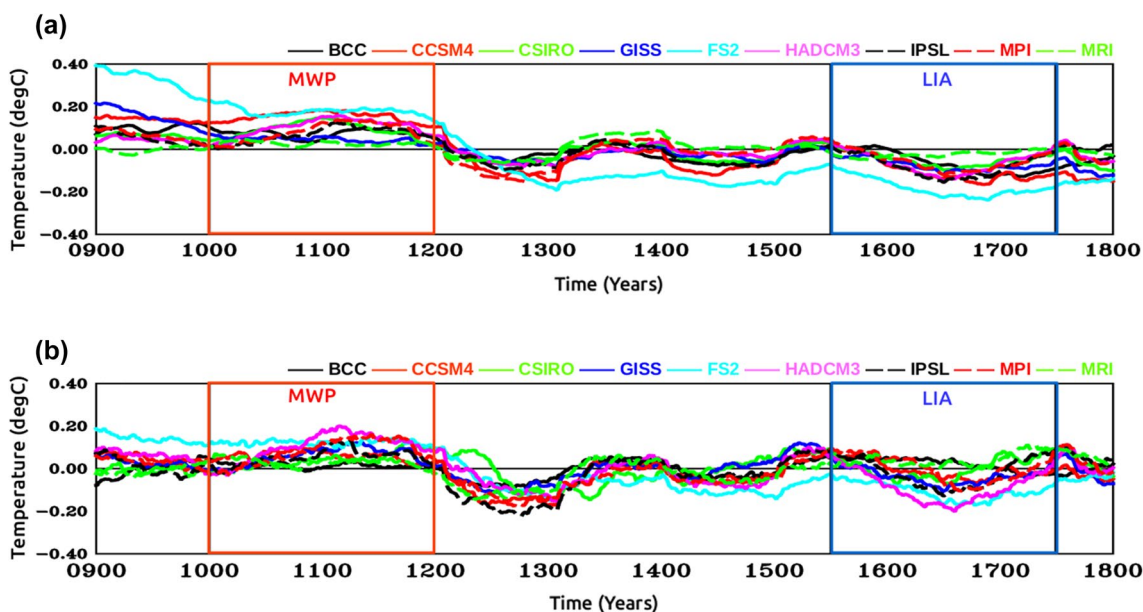


**Fig. 4** 101-year running mean anomalies of near surface air temperature ( $^{\circ}\text{C}$ ) obtained by area-averaging **a** globally, **b** over the Indian Region; The MWP & LIA period are shown in red and blue boxes, respectively

see models showing a warming signal during the MWP (CE 1000–1199) and cooling during the LIA (CE 1550–1749), in a general agreement with the earlier studies (e.g. Fig. 1b of TS-IPCC13). Interestingly, in addition to these two well-known epochs, we see a few more warm and cold climatic periods, but with a shorter duration.

The spread at the time series of  $T_1$  in different models (Figure A3b) is slightly more compared to that for the  $T_G$  (Figure A3a). The temporal anomalies of  $T_1$  are more coherent across these models. Figures A3b and 4b also show that the intermodel-spread in the anomalies of  $T_1$  is relatively less as compared to the corresponding anomalies of  $T_G$ . The sharp cooling around CE 1250 seen in the global summer temperature across the models is simulated over the Indian region as well (Fig. 4a, b), and is coincident with a strong volcanic event, identified as Samalas volcanic eruption (Sigl et al. 2015, Vidal et al. 2016; Gao et al. 2008). In this context, it is worth noting that other volcanic eruptions resulted in potentially decades-long cooling episodes (Liu et al. 2016; Sigl et al. 2015; Iles et al. 2014). Such a signal is apparent from a few proxy records as well (e.g. Fig. 1 TS5 of TS-IPCC13). Also evident is that all the modelled temperatures have apparently entered a cooling phase from this point. We show a proxy record from north India (33°N, 76°E; adapted from Yadav et al. 2009) with the model simulations (Figure A3), which indicates a qualitative agreement between the simulations and the proxy records.

The 101-year running averages of the simulated AAISMR anomaly are presented in Fig. 5a. A linear trend analysis of

AAISMR during LM (Fig. 5b) shows a statistically significant (at 0.10 levels) but the moderate decreasing trend in four models throughout the LM, in agreement with findings from several proxy records (e.g. Fig. 8 of Ramesh et al. 2010). Four other models simulate a weak decreasing trend. In contrast, one model (HadCM3) simulates a moderate increasing trend. Figure 5a also shows an inter-model spread in the anomalous evolution of the AAISMR through the MWP. The time series of the multi-model mean AAISMR also shows a long-term decreasing trend in the LM (Fig. 5b). We find that the MWP is marked by relatively higher ISMR as compared to the LM-mean, and the LIA by a relatively low ISMR (Fig. 5). In comparison, as seen in Figures A3b and 4b, the simulated temperature response over India during the MWP and LIA is relatively more coherent across the models, and its evolution qualitatively agrees with the available proxy records (Yadava et al. 2005; Ramesh et al. 2010; Thamban et al. 2007).

In Table 2, we show the simulated correlation coefficients between AAISMT and NINO3.4 index for the LM period, as well as those in the first, middle and the last 500 year period of the LM. Similar correlations between the AAISMR and NINO3.4 index are presented in the Table 3. In general, these simulated NINO3.4-AAISMR correlations are negative, while the corresponding NINO3.4-AAISMT correlations are positive. Importantly, most of the correlations are significant at 0.05 level from a 2-tailed Student's t-test, suggesting that ENSO has been consistently influencing the Indian climate throughout the LM. Multi-century

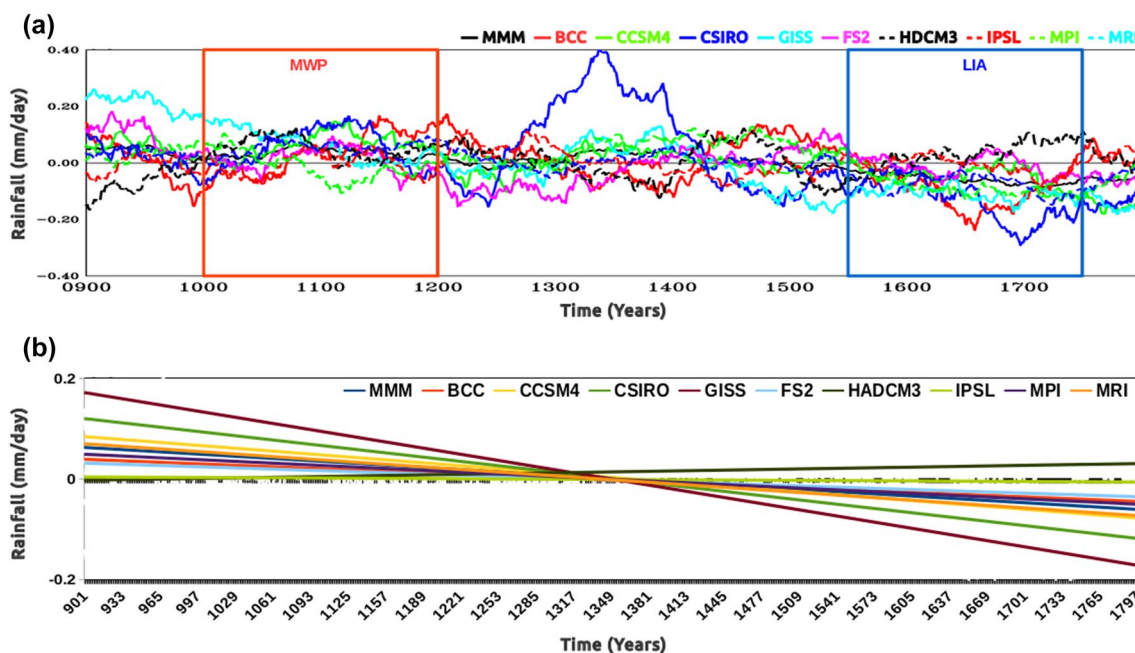


**Fig. 5** **a** 101-year running mean anomalies of ISMR (mm/day); The MWP & LIA period are shown in red and blue boxes, respectively. **b** Linear trend lines of the area-averaged ISMR during LM, as simulated by the nine PMIP3 models

**Table 2** Correlations between NINO3.4 and area-averaged Indian Summer Monsoon surface temperatures (AAISMT) during the Last Millennium, as simulated by CMIP5 models (Significant correlation values are shown in bold and are significant at 0.05 level from 2-tailed student's t-test)

S no	Models	CE 0850–1849	CE 0850–1349	CE 1100–1599	CE 1350–1849
1	BCC	<b>0.26</b>	<b>0.29</b>	<b>0.23</b>	<b>0.23</b>
2	CCSM4	<b>0.31</b>	<b>0.36</b>	<b>0.39</b>	<b>0.26</b>
3	GISS	<b>0.38</b>	<b>0.31</b>	<b>0.38</b>	<b>0.43</b>
4	HADCM3	<b>0.30</b>	<b>0.31</b>	<b>0.30</b>	<b>0.28</b>
5	IPSL	<b>0.59</b>	<b>0.61</b>	<b>0.58</b>	<b>0.58</b>
6	MPI	<b>0.47</b>	<b>0.48</b>	<b>0.49</b>	<b>0.47</b>
7	FS2	<b>0.41</b>	<b>0.44</b>	<b>0.37</b>	<b>0.35</b>
8	CSIRO	<b>0.55</b>	<b>0.53</b>	<b>0.61</b>	<b>0.56</b>
9	MRI	<b>0.47</b>	<b>0.46</b>	<b>0.51</b>	<b>0.47</b>

**Table 3** Correlation between NINO3.4 and area-averaged Indian Summer Monsoon Rainfall (AAISMR) during Last Millennium, as simulated by CMIP5/PMIP3 models (significant correlation values are shown in bold (italic) and are significant at less than 0.05 (0.10) level from 2-tailed student's t-test)

S No	Models	CE 0850–1849	CE 0850–1349	CE 1100–1599	CE 1350–1849
1	BCC	– <b>0.32</b>	– <b>0.34</b>	– <b>0.30</b>	– <b>0.29</b>
2	CCSM4	– <b>0.12</b>	– <i>0.08</i>	– <b>0.11</b>	– <b>0.17</b>
3	GISS	– <b>0.28</b>	– <b>0.24</b>	– <b>0.33</b>	– <b>0.34</b>
4	HADCM3	– <b>0.39</b>	– <b>0.37</b>	– <b>0.37</b>	– <b>0.40</b>
5	IPSL	– <b>0.70</b>	– <b>0.74</b>	– <b>0.69</b>	– <b>0.66</b>
6	MPI	– <b>0.43</b>	– <b>0.43</b>	– <b>0.46</b>	– <b>0.44</b>
7	FS2	– <i>0.05</i>	– <i>0.07</i>	– <i>0.05</i>	– 0.03
8	CSIRO	– <b>0.33</b>	– <b>0.31</b>	– <b>0.32</b>	– <b>0.34</b>
9	MRI	– <b>0.36</b>	– <b>0.32</b>	– <b>0.35</b>	– <b>0.39</b>

model simulation studies by Whittenberg et al. (2009) show multi-decadal changes in the ENSO statistics. The consistent ENSO-monsoon links over a 1000-year simulation across many models as shown above reconfirms that the ENSO is indeed an important driver of the interannual Indian summer monsoon climate variability. However, we must be mindful of the fact that the above analysis only explores the association of an ENSO index with the (AAISMR), which may not necessarily apply to every local region of the Indian region.

### 3.3 MWP and LIA analysis

The simulated interannual standard deviations of JJAS surface temperatures (for both global as well as the Indian regions), the ISMR and the NINO3.4 index during the MWP and LIA periods are presented in Table A4. In five out of nine models, the amplitude of simulated NINO3.4 standard deviations during LIA are lower than those during the MWP, but only marginally so. Standard deviations of other variables across the MWP and LIA only differ marginally.

Simultaneous correlation coefficients between the summer NINO3.4 index with the AAISMR during the MWP and LIA from the individual models are shown in Fig. 6a, and those with the corresponding AAISMT in the Fig. 6b. The signs and magnitudes of all these correlations are comparable to the corresponding correlations from observations during the HS, as well as statistically significant at 0.1 level. In

fact, the simulated area-averaged AAISMR-NINO3.4 index correlations for both MWP and LIA periods, except those for the FGOALS-s2 model, are statistically significant at 0.05 level from a 2-tailed Student's t-test. Notably, for the Indian region, the magnitudes of the correlations with the ENSO index are stronger in the case of the surface temperature as compared to the rainfall (Fig. 6). Interestingly, for five (six) models out of the nine, the magnitudes of the correlation coefficients of the NINO3.4 index with the AAISMR (AAISMT) are weaker in the LIA relative to the corresponding correlations over the MWP.

We also carry out a bootstrapping significance test (1000 simulations) for the AAISMR-NINO3.4 correlation; we find that the results for all nine models are significant at 0.005 level. Further, four out of nine models show weaker magnitude in correlations during the LIA relative to the MWP (Fig. 7a). These correlations indicate a strong multi-decadal-through-centennial modulation of the association between the ENSO and ISM during LM. The difference of AAISMR-NINO3.4 correlations between the MWP and LIA in four models (CCSM4, CSIRO, IPSL and MRI) is statistically significant at 0.10 level, as seen from the bootstrapping tests (Fig. 7b).

To explore this aspect further, we present the simulated frequencies of 'strong' El Niños and La Niñas during the MWP and LIA by the individual models in Table 4. For this calculation, we catalogue a simulated ENSO event as

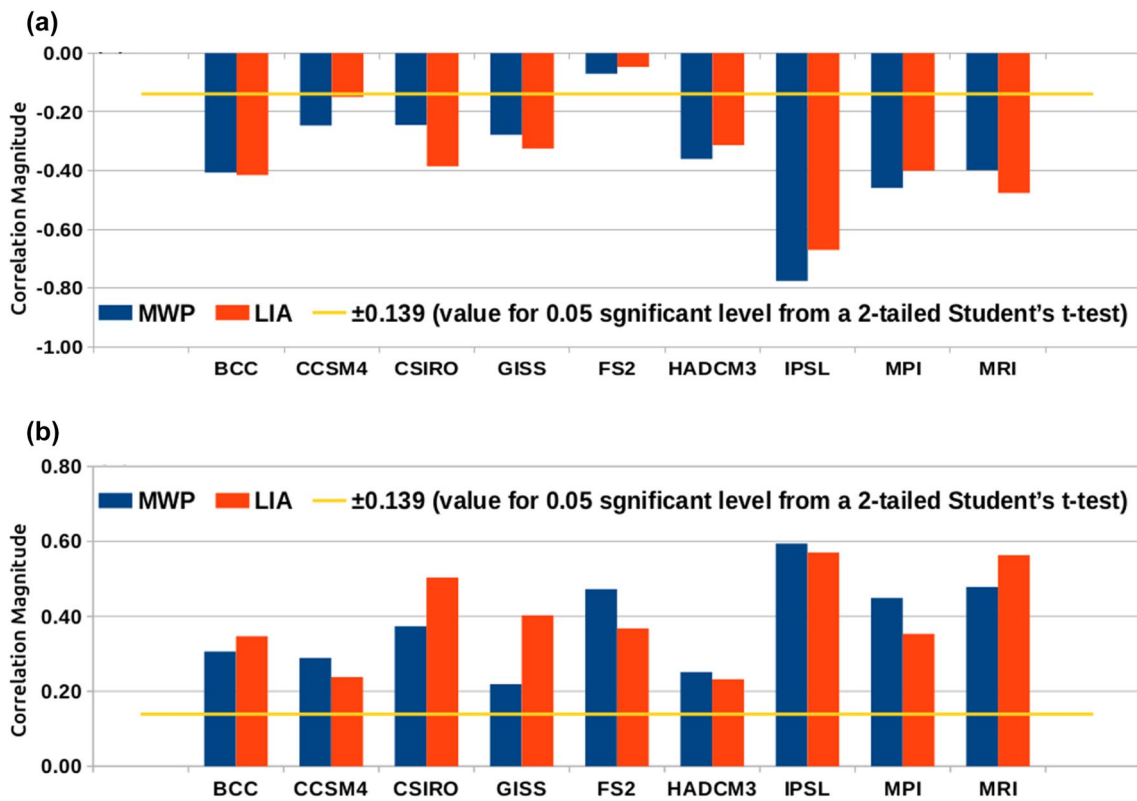


Fig. 6 Simulated correlations, for each model, during MWP (blue bars) and LIA (red bars) between the NINO3.4 index and a AAISMR, and b AAISMT. Yellow line shows the significant value at 0.05 level from a 2-tailed Student's t-test

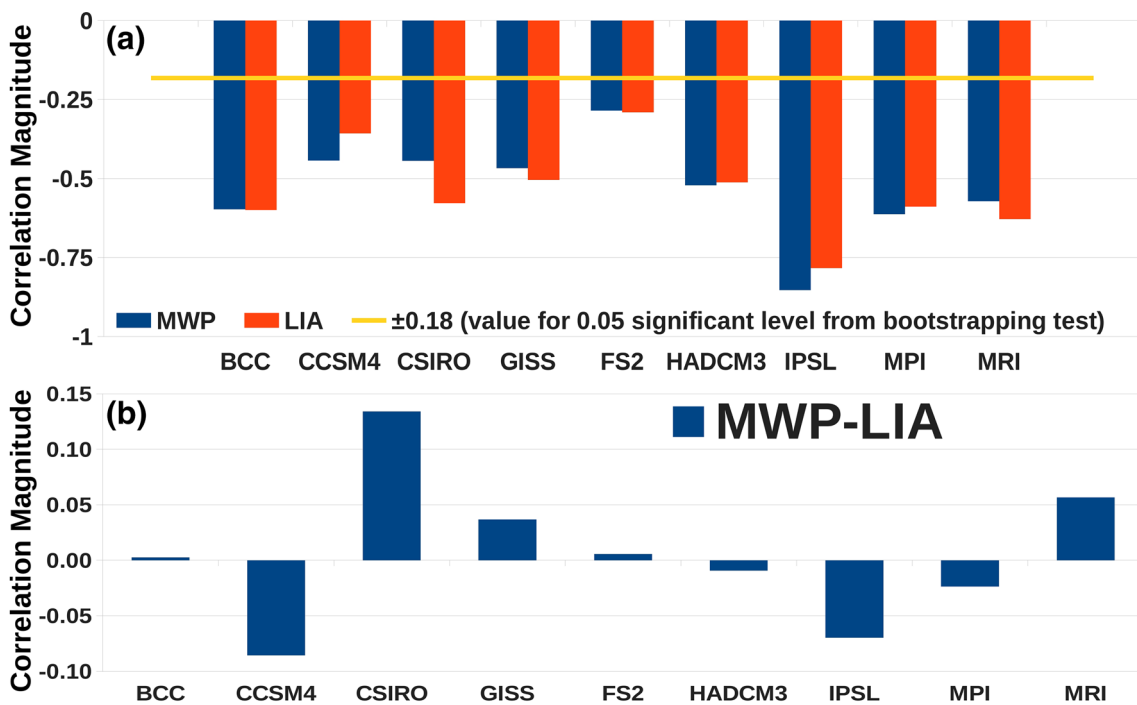


Fig. 7 a Bootstrapping correlations (for 1000 simulations) during MWP (blue bars) and LIA (red bars) for individual respective models. b Bootstrapping correlation difference between MWP and LIA (MWP-LIA; for 1000 simulations). In panel a, 0.18 represents the statistically significant correlation from this test, significant at 0.05 significance level

**Table 4** Categorization of El Niños and La Niñas as per the normalized strength of the NINO3.4 index of each particular ENSO. ‘ $\sigma$ ’ in the following table represents the standard deviation of the NINO3.4 index

S. No	El Niño classification		La Niña classification	
1	$> 0.5\sigma < 1\sigma$	Weak El Niño	between $(-1\sigma$ and $-0.5\sigma)$	Weak La Niña
2	$> 1\sigma$	Strong El Niño	$< -1\sigma$	Strong La Niña

strong when the amplitude of the NINO3.4 index exceeds one standard deviation i.e. ‘ $1\sigma$ ’ (Table 5). The majority of models consistently simulates more number of strong El Niños in MWP as compared to the number of strong El Niños in LIA, and the majority of models consistently simulates more number of strong La Niñas in LIA as compared to the number of strong La Niñas in MWP, as shown in the Table 5; this result is statistically significant at 0.05 level from a two-tailed Student’s t-test carried out for difference of means. Interestingly, a majority of the PMIP3 models (six) simulate more strong El Niños as compared to strong La Niñas during the MWP (Table 5). On the other hand, the number of strong La Niñas is marginally more than that of strong El Niños in seven models during the LIA. This clearly shows, strong El Niños are more dominant in the tropical Pacific during MWP in majority of the models and ‘strong’ La Niñas are more dominant in the tropical Pacific during the LIA.

We also show the simulated multi-model mean (MMM) SST differences of the MWP from that of the LM, along with the corresponding anomalous SST for the LIA relative the LM, in Figures A5, which shows that the tropical SST were relatively warmer (cooler) during the MWP (LIA).

The background changes in temperatures may modulate the relative strengths of El Niños and La Niñas (e.g. Federov & Philander 2000). This may be a possible cause for more strong El Niños in MWP and La Niñas in LIA. On the other hand, in the recent period, El Niños and La Niñas have been suggested to cause an anomalous increase and decrease in global temperature, respectively (e.g. Trenberth et al. 2002).

Importantly, a study using a Cane-Zebiak type of coupled model (Mann et al. 2005) suggests La Niña-like conditions during the MWP. In this context, it is pertinent to note that several proxy based studies (Cobb et al. 2003; Graham et al. 2007; Mann et al. 2009) suggest either a weak ENSO variance, or more La Niñas during the MWP. A study by Henke et al. (2017) based on precipitation proxy data compilation shows a propensity of more El Niño-like LIA compared to the MWP; however as per Henke et al. (2017), the difference is not statistically significant and, is not apparent in a proxy-derived temperature compilation. On the other hand, a study by Conroy et al. (2008), finds that their diatom record is not consistent with the SST interpretation with that of a coral record (Cobb et al. 2003). Specifically, while the diatom record suggests warmer SST in the eastern equatorial Pacific during some part of the medieval period, the coral derived SST indicates a cooling trend in the same location. Conroy et al. (2008) suggest a more heterogeneous SST in the region. Notably, Henke et al. (2017) claim that their result is insensitive to the choice of definition for the MWP and LIA. Therefore, a higher number of the PMIP3-simulated El Niños as compared to La Niñas in almost all the models during the MWP is supported to a good extent by Conroy et al. (2008)’s observations, and agrees reasonably well with the proxy-temperature analysis of Henke et al. (2017).

Given this agreement across the models, which have a more detailed oceanic component as compared to simpler models such as that used in Mann et al. (2005), the relevance of any positive skewness in ENSOs for global temperature during the MWP (as against the influence of external

**Table 5** Frequency table of simulated El Niños and La Niñas during MWP (CE 1000–1199) and LIA (CE 1550–1749)

S No	Models	MWP (CE 1000–1199)				LIA (CE 1550–1749)			
		Weak El Niños	Strong El Niños	Weak La Niñas	Strong La Niñas	Weak El Niños	Strong El Niños	Weak La Niñas	Strong La Niñas
1	BCC	47	33	20	36	41	29	31	35
2	CCSM4	25	45	21	24	37	27	29	29
3	GISS	32	42	25	30	34	28	23	41
4	HADCM3	38	41	35	23	26	23	31	34
5	IPSL	42	32	22	34	36	23	26	40
6	MPI	29	40	32	26	36	33	32	39
7	CSIRO	53	35	69	30	63	34	64	32
8	MRI	64	27	70	32	73	31	61	30
9	FS2	39	41	27	30	27	27	43	35

forcing) needs to be verified by making some AGCM sensitivity experiments, which we plan to do in near future.

Despite the statistically significant correlations between the simulated AAISMR-NINO3.4 index, it will be interesting to explore any non-linearity in the association. When averaged over the nine models, the percentage of strong El Niño events with concurrent negative AAISMR anomalies (henceforth referred to as  $EL^-$ ) is about 69 and 77 during the MWP and LIA, respectively (Table 6; Fig. 8). To be specific, five models simulate a significantly higher proportion of  $EL^-$  during the LIA (90%, 78%, 85%, 87% and 82% of strong El Niños in LIA) as compared to those in MWP (70%, 51%, 63%, 70% and 68% of El Niños in MWP). Other models simulate an almost equal number (up to a difference of 1%) of  $EL^-$ . Thus, we can say that the simulated strong El Niños during the LIA tend to be more ‘efficient’ as compared to those in MWP in causing negative ISMR anomalies.

On the other hand, it is evident from the Table 6, the model-averaged percentage of strong La Niñas with positive AAISMR anomalies (referred to as  $LN^+$ ) shows a higher percentage during MWP (70%) than that during the LIA (62%). Five models simulate significantly higher numbers of  $LN^+$ , among all La Niñas during MWP (75%, 71%, 97%, 57%, 70%, 81% and 50%) as compared to those in LIA (68%, 55%, 91%, 33%, 59%, 70% and 43%). One model simulates an almost equal number of  $LN^+$ . Therefore, we infer that the simulated strong La Niñas are apparently more ‘efficient’ in causing positive AAISMR anomalies during MWP relative to those in LIA.

The above results indicate the propensity of the simulated El Niños during the LIA and La Niñas during the MWP to be relatively more ‘efficient’ in delivering the canonical impact on the summer monsoon rainfall in India, notwithstanding

the statistically significant NINO3.4-AAISMR correlations (Fig. 6a). This suggests a possibility of background changes modulating the interannual Indian summer monsoon rainfall-ENSO association. These slow background changes counter the El Niño impacts in several local regions of India. This is the reason why we have a relatively high rainfall over India despite having more El Niños, and the ENSO correlation with the area-averaged rainfall being moderately negative, but still statistically significant.

### 3.4 Possible dynamics involved

We present the results from analysis of multi-model mean and other two representative models in Fig. 9 to delineate, the possible dynamics behind the relatively higher rainfall during the MWP and lesser rainfall during the LIA over India. Prior to that, we shall briefly ensure that the models qualitatively reproduce the observed zonal convergence-divergence zones associated with the Walker circulation in the tropical Pacific. The variability of the Walker circulation, is critical for transferring the ENSO impacts on climate elsewhere beyond the eastern tropical pacific.

The large scale Walker circulation is illustrated by the distribution of the anomalous JJAS velocity potential at the 850 hPa ( $\chi_{850}$ ) from the NCEP observational analysis for the period CE 1948–2005 and the HS qualitatively similar and models are able to simulate the NCEP-NCAR reanalysis convergence-divergence pattern in the tropical Pacific for the 1948–2005 period (figures not shown).

Note that, as far as the Fig. 9 is concerned, the term ‘difference/differential’ for any parameter during the MWP (LIA) refers to the excess/deficit of the said parameter during the MWP (or LIA) as compared to that for the LM.

**Table 6** Percentages of ‘strong’ (a) El Niños with positive ( $EL^+$ ) and negative ( $EL^-$ ) area-averaged ISMR anomalies, and (b) La Niñas with positive ( $LN^+$ ) and negative ( $LN^-$ ) area-averaged ISMR anomalies during both MWP and LIA

Models	MWP $EL^+$	LIA $EL^+$	MWP $EL^-$	LIA $EL^-$	MWP $LN^+$	LIA $LN^+$	MWP $LN^-$	LIA $LN^-$
BCC	30	10	70	90	75	68	25	31
CCSM4	33	44	67	55	71	55	29	45
GISS	29	21	79	78	56	58	43	41
HADCM3	49	22	51	78	69	76	30	23
IPSL	00	13	100	87	97	91	3	8
MPI	32	18	68	82	57	33	42	67
CSIRO	37	15	63	85	70	59	30	38
MRI	30	13	70	87	81	70	19	30
FS2	44	48	56	52	50	43	50	57
AVERAGE	32	23	69	77	70	62	30	38

Positive (+)=Positive anomalies of area-averaged ISMR (AAISMR)

$EL^{+(-)}$ =Positive (negative) AAISMR Anomalies associated with El Niños

$LN^{+(-)}$ =Positive (negative) AAISMR Anomalies associated with La Niñas

Negative (–)=Negative anomalies of area-averaged ISMR (AAISMR)

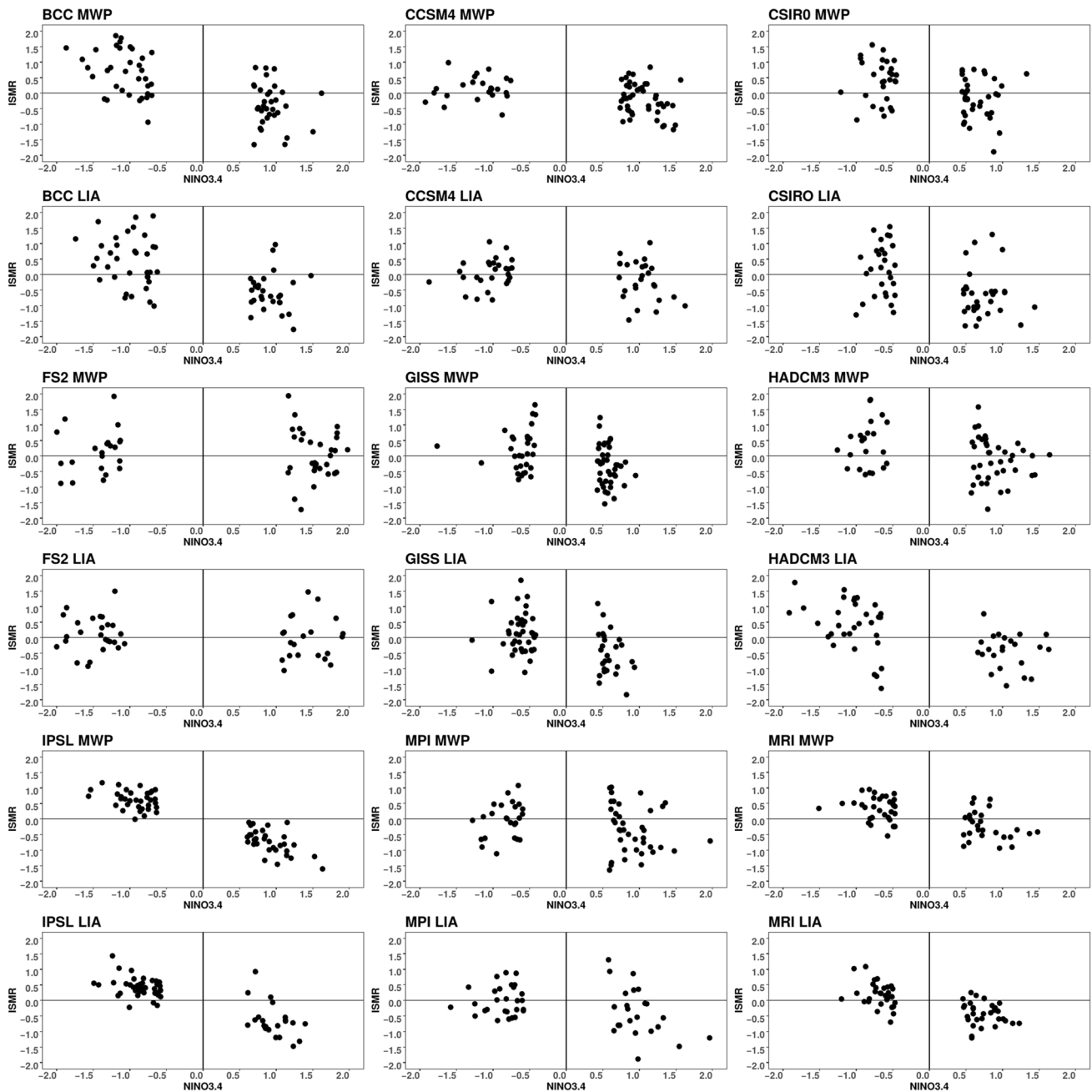
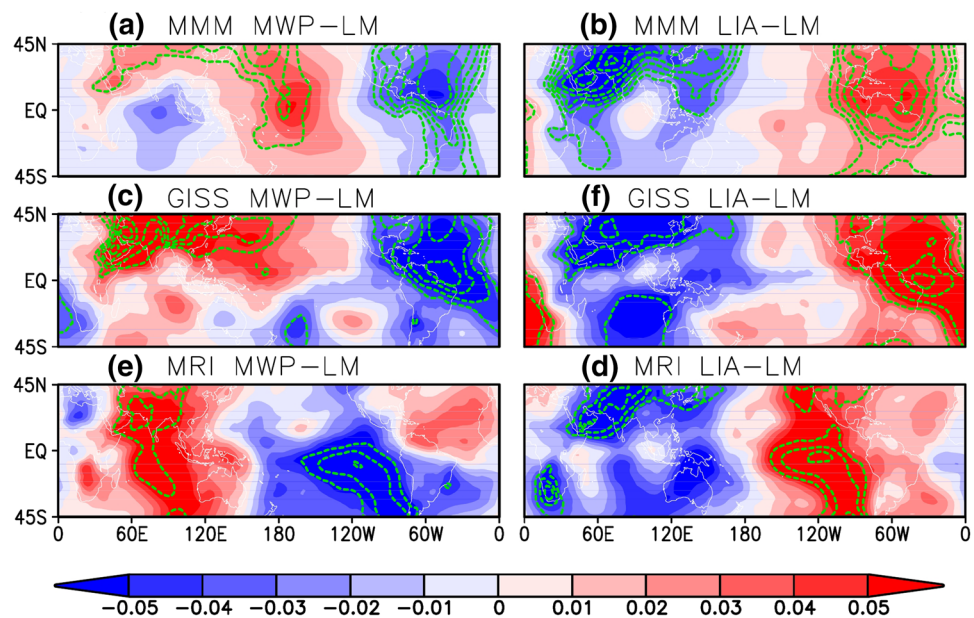


**Fig. 8** Scatter plots showing simulated NINO3.4 index ( $^{\circ}\text{C}$ ) on the X-Axis and simulated area-averaged ISMR (mm/day) on Y-Axis during both MWP and LIA. The last descriptor string in each panel indicates the name of the model and the period

That is, i.e.  $P_{\text{MWP}} - P_{\text{LM}}$ , for example,  $P$  being any climate variable such as the rainfall. From the distribution of different fields in boreal summer  $\chi_{850}$  simulated by models shown in Fig. 9, we see a zone of excess convergence in the central tropical Pacific, flanked by two zones of excess divergence in the equatorial Pacific during the MWP relative to the LM, suggesting a relative westward shift in the Walker circulation during the MWP. We also see a similar shift relative to the simulations from the historical

period (Fig. 9). This may suggest a background change during the MWP as compared to the LM, and other sub-periods such as the LIA. Importantly, the simulated excess divergence centre in the western Pacific, extends into the equatorial eastern Indian Ocean, which we believe results in an excess convergence zone over India during the MWP relative to the LM (Fig. 9), and therefore excess rainfall during the MWP as compared to the LM. The differential convergence patterns of the large-scale circulations during

**Fig. 9** Distributions of simulated 850 hPa differences in the time-averaged JJAS velocity potential  $\chi_{850}$  ( $\text{m}^2 \text{s}^{-1}$ ) differences. The descriptor string above each panel indicates the name of the model and the periods over which the difference is calculated. The top left panel, for example shows the GISS model simulated excess of mean JJAS  $\chi_{850}$  ( $\text{m}^2 \text{s}^{-1}$ ) as compared to that for the LM. Statistical significance at 80% confidence level from Student's t-test is showed in contours



the MWP and LIA relative to the historical period (Figures not shown) are qualitatively similar to the anomalous patterns relative to the LM (Fig. 9). Seven models simulate moderately excessive convergence over India during MWP relative to Historical period, while six models simulate surplus divergence over India during the LIA.

From Figure A5, we can conjecture that there is an association in the aforementioned circulation changes with those in the SST, for example, an increase in low level convergence of zonal winds over the central equatorial pacific during the MWP associated with a concurrent increase in the SST relative to the LM mean condition (Fig. 9a, Figure A5a).

The composite spatial distribution of rainfall anomalies over the Indian domain are statistically significant at 0.10 level from a 2-tailed Student's t-test (Fig. 10). Having said this, as a majority of the models indicate a similar sign of anomalies in major portions of the region, the results may qualitatively be considered as conforming across these models. We also see a modest warming across the Indian region

in all simulations of the MWP (Figures not shown) in agreement with Fig. 4b.

The 850 hPa convergence distribution relative to that during the LM (Fig. 9) suggests stronger convergence in the eastern tropical Pacific compared to the LM. An anomalous divergence center over India results in relatively lesser rainfall during the LIA compared to both MWP and LM. From this, it is evident that there is a shift in large-scale Walker circulation patterns.

Importantly, we also find an general increase in the simulated specific humidity during MWP, particularly over the tropics (Fig. 11). This may indeed be due to increase in temperature during MWP. We also find an anomalous increase in the simulated moisture transport into the Indian region during summer monsoon, mostly significant during both the MWP and LIA (Fig. 11). The increased background convergence over India (Fig. 9) during the MWP may also facilitated this inward excess of background moisture transport. This, along with an increases in local moisture retained

**Fig. 10** Shaded regions represent the extent of statistically significant (at 90% confidence level) composite **a** rainfall anomalies, and **b** surface temperature. The statistically significance has been ascertained using a 2-tailed Student's t-test

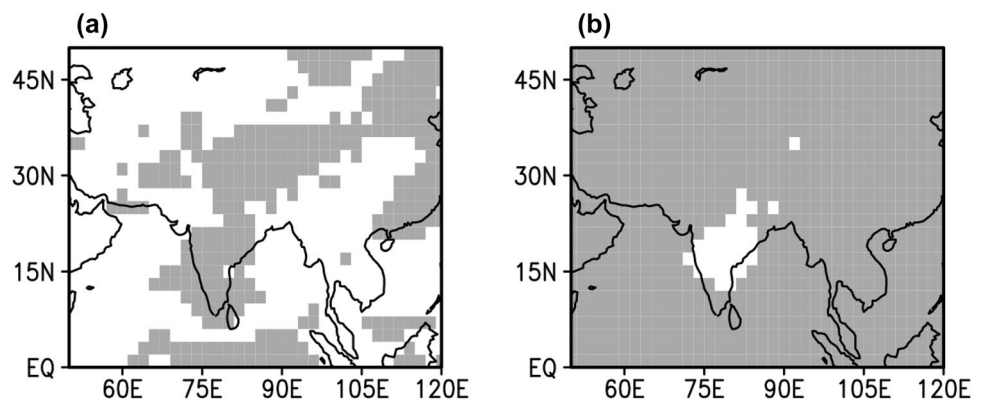
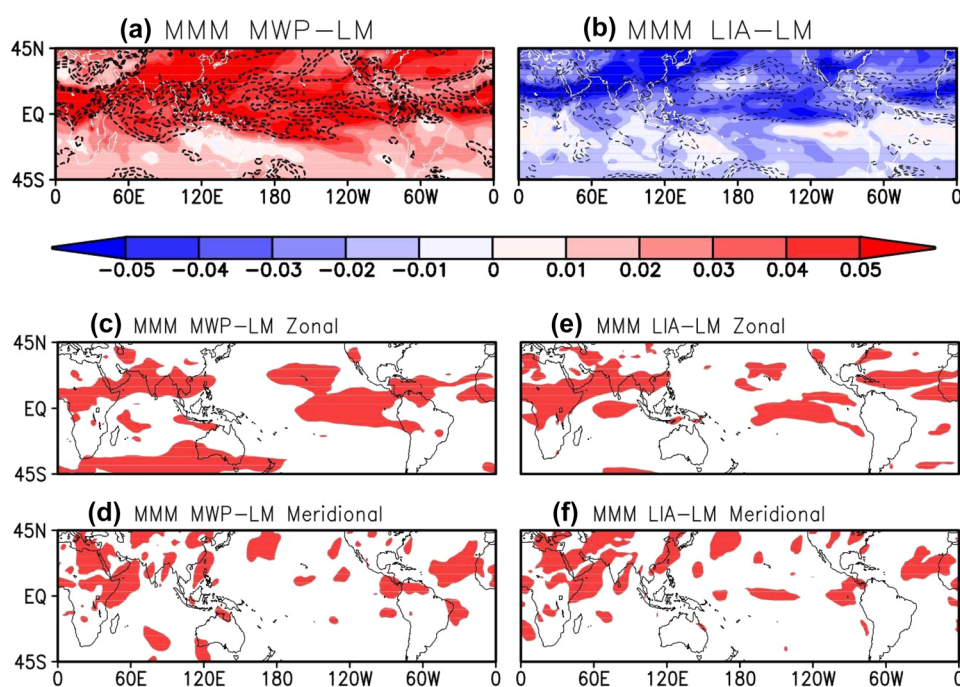


**Fig. 11** Distributions of simulated differences in the multi-model mean 850 hPa JJAS specific humidity for **a** MWP and **b** for LIA. Statistically significant differences at 95% confidence level from a two-tailed Student's t-test are marked with black contour lines. Panels **c–f** show the distributions of simulated zonal and meridional extents of moisture transport at 850 hPa that are significant at 90% confidence level from a two-tailed Student's t-test. The descriptor string above each panel indicates the periods over which the difference is calculated for the multi-model mean (MMM)



in the atmosphere owing to the increasing temperatures (Fig. 11a), may have resulted in a relative increases in ISMR during the MWP.

#### 4 Conclusions and scope for future studies

The global climate has experienced significant centennial climate variability in the last two millennia (IPCC 2013). Proxy-data based studies identify two significant periods in the last millennium (LM): (1) a relatively warm period known in the literature as the ‘Medieval Warm Period’ (MWP, CE 950–1350) followed roughly after 150–200 years by (2) a relatively cooler period referred to as the Little Ice Age (LIA, CE 1500–1850). Notably, variability of the ISM in reference to the above mentioned climatic events is relatively less studied. While a few proxy records document such periods in the Indian region, the paucity of data introduces uncertainty in quantifying the climate state parameters during those events.

To complement the proxy-studies, we carry out an analysis of the available PMIP3 data sets from nine models. We find that all the models simulates the warming (MWP) and cooling (LIA) temperatures during epochs CE 1000–1199 and CE 1550–1749 roughly commensurate with the proxy-observations.

A majority of the models qualitatively reproduces a wetter (drier) Indian summer monsoon season in the MWP (LIA) relative to the mean Indian summer monsoon during the LM. The models simulate a statistically significant ENSO-Monsoon association during the LM in similar to

the current day climate. Interestingly, we find a propensity of the simulated strong El Niños (La Niñas) during the LIA (MWP) having a relatively more ‘efficient’ canonical impact, notwithstanding the statistically significant NINO3.4-ISM correlation. Importantly, most models simulate more ‘strong’ El Niños during MWP as compared to ‘strong’ La Niñas. And also, most models simulate more ‘strong’ La Niñas during the LIA as compared to ‘strong’ El Niños. Despite such a relatively high occurrence of strong El Niños relative to the LIA, a relatively westward shift in the simulated anomalous summer Walker circulation as compared to the mean LM condition. This change in background circulation is apparently associated with a simulated background change in the tropical Indo-pacific SST, in most of the models. The multi-decadal/centennial shift Walker circulation is reflected in an apparent anomalous divergence in the equatorial eastern Indian Ocean during the MWP, which in turn results in concurrent anomalous convergence and excess rainfall in the Indian region. Some model studies (e.g. Ashok et al. 2004) indicate that a presence of anomalous low level divergence in the eastern equatorial Indian Ocean is critical in causing an anomalous divergence over the peninsular Indian region and thereby leading to less than mean rainfall there. All this suggests a modulation of the interannual ISMR-ENSO associated with slow background changes. It is reasonable that the convergence/divergence patterns in the eastern equatorial Indian Ocean, which is more of a peripheral region for ENSO impact, may change depending on the background changes in circulation. Importantly, the relative increase in the simulated ISMR during the MWP is

also associated with an increase in specific humidity, and increased moisture transport into the Indian region during the MWP.

The simulated surface temperature over India is only modestly higher during MWP as compared to the corresponding LM average, owing to the spread of the signals across the models. A plausible reason, which has not been ascertained in this study, is whether the simulated Indian summer rainfall during the MWP mostly comes from a number of extreme rainfall events as compared to the LM-average, a situation somewhat analogous to warmer and wetter scenario due to the increased saturated water vapour associated with increased temperature in the background of global warming (e.g. Lehmann et al. 2015; Goswami et al. 2006). One also needs to be sensitive to the plausibility that at least some of the changes in the Indian climate (and such changes in several other regions) during the LM may also be due to 'direct' impacts of the changes in the radiative forcing through the LM, rather than just due to the 'internal' variability such as the changing ENSO characteristics. We plan to conduct a suite of atmospheric GCM experiments in addition to some specially designed coupled experiments in this connection. Apart from this, we also plan to analyse the future scenarios to identify any analogous or contradicting scenarios to those we see in the PMIP3.

In this manuscript, we also carry out an analysis of the changes in the simulated pre-monsoon and monsoonal season temperature gradient between the area-averaged land temperatures in the Indian region and the Indian ocean to its south. While the results suggest a weakening of such temperature gradient from the MWP to the LIA in majority of the models, the changes are very weak in magnitude.

Our results, of course are subject to the model uncertainties and inter-model spread. Having said this, an agreement across a majority of the models, and the agreement with the findings from available proxy data, gives us confidence in the results. It will be interesting to examine, in more detail, the mechanism/reasons for the simulated distinct summer Walker circulation signatures in the tropical Indian ocean during the MWP & LIA, and delintate the relative contributions of local increase in moisture over India due to the increased warming in MWP and that transported inward due to the circulation changes. Another important aspect that we hope to study is to explore whether the models are able to simulate the shrinking of the 'Indo-Pacific' rain belt during the LIA as documented in Denniston et al. (2016) from proxy-data sets, and if they do, whether such a shrinking has a role to play in the changed ENSO-Monsoon links, at least in the model world.

**Acknowledgements** KA, SC, and CTT thank the contribution of Prof. Rengaswamy Ramesh, their co-author who sadly passed away on 2 April 2018. We thank Dr. Johann H. Jungclauss, the Max Planck

Institute for Meteorology (MPI-M) Hamburg for sharing the model outputs. Constructive comments from two anonymous reviewers helped to improve the manuscript. The GrADS, Ferret, and NCL graphics tools, and the CDO statistical software have been used in this study. KA and SC acknowledge the Climate Change programme (SPLICE) of the Department of Science and Technology, Government of India, for grant No. DST/CCP/NCM/76/2017(G) for this research. CTT acknowledges a PhD fellowship grant from the UGC, Govt. of India to carry out this work.

**Data Availability** Model simulation outputs have been downloaded and available from "<http://cera-www.dkrz.de/WDCC/ui/Index.jsp>" and "<https://esgf-index1.ceda.ac.uk/search/cmip5-ceda/>". The GPCP, CMAP, NCAR Reanalysis 1 datasets are freely available at NCAR-ESRL archive <<https://www.esrl.noaa.gov/psd/data/gridded/>>. The HadISST dataset is freely available from Met Office Hadley Centre observations datasets archive <<https://www.metoffice.gov.uk/hadobs/hadisst/>>. The ECMWF ERA-20CM datasets can be downloaded from their data archive <<https://www.ecmwf.int/en/forecasts/datasets/reanalysis-datasets/era-20cm-model-integrations>>.

## References

- Adler RF, Huffman GJ, Chang A, Ferraro R, Xie P, Janowiak J, Rudolf B, Schneider U, Curtis S, Bolvin D, Gruber A, Susskind J, Arkin P, Nelkin E (2003) The version 2 global precipitation climatology project (GPCP) monthly precipitation analysis (1979-present). *J Hydrometeor* 4(6):1147–1167
- Ashok K, Guan Z, Yamagata T (2001) Impact of the Indian Ocean dipole on the relationship between the Indian monsoon rainfall and ENSO. *Geophys Res Lett* 28(23):4499–4502
- Ashok K, Guan Z, Saji NH, Yamagata T (2004) Individual and combined influences of ENSO and the Indian Ocean dipole on the Indian summer monsoon. *J Climate* 17(16):3141–3155
- Ashok K, Behera S, Rao AS, Weng HY, Yamagata T (2007) El Niño Modoki and its teleconnection. *J Geophys Res* 112:C11007. <https://doi.org/10.1029/2006JC003798>
- Behera SK, Krishnan R, Yamagata T (1999) Unusual ocean-atmosphere conditions in the tropical Indian Ocean during 1994. *Geophys Res Lett* 26:3001–3004
- Berkehammer M, Sinha A, Mudelsee M, Cheng H, Edwards RL, Cannariato K (2010) Persistent multidecadal power of the Indian Summer Monsoon. *Earth Planet Sci Lett* 290:166–172
- Berkehammer M, Sinha A, Stott L, Cheng H, Pausata FSR, Yoshimura K (2012) An abrupt shift in the Indian monsoon 4000 years ago. *Geophys Monogr Ser* 198:75–87
- Cai W et al (2015) ENSO and greenhouse warming. *Nature Clim Change* 5:849–859
- Chakraborty S, Goswami BN, Dutta K (2012) Pacific coral oxygen isotope and the tropospheric temperature gradient over Asian monsoon region: a tool to reconstruct past Indian summer monsoon rainfall. *J Quat Sci* 27(3):269–278. <https://doi.org/10.1002/jqs.1541>
- Cobb KM, Charles CD, Cheng H, Edwards RL, El Niño/Southern Oscillation and tropical Pacific climate during the last millennium: *Nature*. Vol. 424, no. 6946, pp. 271–276
- Collins M (2000) The El Niño Southern Oscillation in the Second Hadley Centre Coupled Model and Its Response to Greenhouse Warming, (1997), 1299–1312
- Conroy JL, Restrepo, Alejandra, Overpeck JT, Steinitz-Kannan M, Cole JE, Bush MB, Colinvaux PA, Unprecedented recent warming of surface temperatures in the eastern tropical Pacific Ocean,

- 2008/12/21/online,v1-2, Nature Publishing Group, <https://doi.org/10.1038/ngeo390>
- Denniston Rhawn F, Caroline C, Ummerhofer AD, Wanamaker MS, Lachniet G, Villarini Y, Asmerom VJ, Polyak, Kristian J, Passaro J, Cugley D, Woods, William F, Humphreys (2016) Expansion and contraction of the Indo-Pacific Tropical Rain Belt over the Last Three Millennia, *Scientific Reports* 6. <https://doi.org/10.1038/srep34485>
- DiNezio Pedro N, Gabriel A, Amy C (2013) Detectability of changes in the walker circulation in response to global warming. *J Clim*. <https://doi.org/10.1175/JCLI-D-12-00531.1>
- Dixit Y (2013) Holocene monsoon variability inferred from paleo-lake sediments in North-western India PhD thesis University of Cambridge, UK
- Dixit Y, Tandon SK (2016) Earth-science reviews hydroclimatic variability on the Indian subcontinent in the past millennium? Review and assessment. *Earth-Sci Rev* 161:1–15. <https://doi.org/10.1016/j.earscirev.2016.08.001>
- Dixit Y, Hodell DA, Petrie CA (2014a) Abrupt weakening of the summer monsoon in northwest India ~ 4100 year ago. *Geology* 42:339–342
- Dixit Y, Hodell DA, Sinha R, Petrie CA (2014b) Abrupt weakening of the Indian summer monsoon at 8.2 kyr B.P. *Earth Planet. Sci Lett* 391:16–23
- Dixit Y, Hodell D, Sinha R, Petrie C (2015) Oxygen isotope analysis of multiple, single ostracod valves as a proxy for combined variability in seasonal temperature and lake water oxygen isotopes. *J Paleolimnol* 53:35–45
- Dutt S, Gupta AK, Clemens SC, Cheng H, Singh RK, Kathayat G, Edwards RL (2015) Abrupt changes in Indian summer monsoon strength during 33,800 to 5500 years BP. *Geophys Res Lett* 42:5526–5532
- Emile-Geay J, Cane M, Seager R, Kaplan A, Almasi P (2007) El Niño as a mediator for the solar influence on climate. *Paleoceanography* 22:PA3210. <https://doi.org/10.1029/2006PA001304>
- Feba F, Ashok K, Ravichandran M, (2018), Role of changed Indo-Pacific atmospheric circulation in the recent disconnect between the Indian summer monsoon and ENSO. *Clim Dyn*. <https://doi.org/10.1007/s00382-018-4207-2>
- Fedorov AV, Philander SG (2000) Is El Niño changing? *Science* 288:1997–2002
- Fleitmann D, Burns SJ, Mudelsee M, Neff U, Kramers J, Mangini A, Matter A (2003) Holocene forcing of the Indian monsoon recorded in a stalagmite from southern Oman. *Science* 300:1737–1739
- Fleitmann D, Burns SJ, Mangini A, Mudelsee M, Kramers J, Villa I, Neff U, Subbary A-A, Buettner A, Hippler D, Matter A (2007) Holocene ITCZ and Indian monsoon dynamics recorded in stalagmites from Oman and Yemen (Socotra). *Quat Sci Rev* 26:170–188
- Gao C, Robock A, Ammann C (2008) Volcanic forcing of climate over the past 1500 years: An improved ice core-based index for climate models. *J Geophys Res* 113:D23111
- Goswami BN, Venugopal V, Sengupta D, Madhusoodanan MS, Xavier PK (2006) Increasing trend of extreme rain events over India in a warming environment. *Science* 314(5804):1442–1445
- Graham NE, Hughes MK, Ammann CM, Cobb KM, Hoerling MP, Kennett DJ, Kennett JP, Rein B, Stott L, Wigand PE, Xu T (2007) Tropical Pacific mid-latitude teleconnections in medieval times. *Clim Change* 83:241–285
- Graham NE, Ammann CM, Fleitmann D, Cobb KM, Luterbacher J (2010) Support for global climate reorganization during the Medieval Climate Anomaly. *Clim Dyn* 37:1217–1245
- Grove JM (1988) *The Little Ice Age*. Methuen, London
- Guhathakurta P, Rajeevan M (2008) Trends in the rainfall pattern over India. *Int J Climatol* 28:1453–1469. <https://doi.org/10.1002/joc.1640>
- Gupta AK, Anderson DM, Overpeck JT (2003) Abrupt changes in the Asian southwest monsoon during the Holocene and their links to the North Atlantic Ocean. *Nature* 421:354–357
- Henke Lilo MK, Hugo Lambert F, Dan J Was the Little Ice Age more or less El Niño-like than the Medieval Climate Anomaly? Evidence from hydrological and temperature proxy data. *Clim Past*, 13, 267–301 2017 <http://www.clim-past.net/13/267/2017/> <https://doi.org/10.5194/cp-13-267-2017>
- Hersbach H (2015) ERA-20CM: a twentieth-century atmospheric model ensemble, (July), 2350–2375. <https://doi.org/10.1002/qj.2528>
- Iles CE, Hegerl GC (2014) The global precipitation response to volcanic eruptions in the CMIP5 models. *Environ Res Lett* 9(10):104012
- IPCC (2013) *The Physical Science Basis. Contribution of Working Group I to the Fifth Assessment Report of the Intergovernmental Panel on Climate Change* [Stocker, In: Qin TF,D, Plattner G-K, Tignor M, Allen SK, Boschung J, Nauels A, Xia Y, Bex V, Midgley PM (eds.) *Climate Change 2013*. Cambridge University Press, Cambridge, 1535 pp. <https://doi.org/10.1017/CBO9781107415324>
- Kalnay et al (1996) The NCEP/NCAR 40-year reanalysis project. *Bull Amer Meteor Soc* 77:437–470
- Keshavamurthy RN (1982) Response of the atmosphere to sea surface temperature anomalies over the equatorial Pacific and the teleconnections of the Southern Oscillation. *J Atmos Sci* 39:1241–1259
- Kitoh A (2007) Variability of Indian monsoon-ENSO relationship in a 1000-year MRI-CGCM2.2 simulation. *Nat Hazards* 42(2):261–272. <https://doi.org/10.1007/s11069-006-9092-z>
- Kripalani RH, Kulkarni A (1999) Climatological impact of El Niño/La Niña on the Indian monsoon: a new perspective. *Weather* 52:39–46
- Krishnan R, Sabin TP, Vellore R, Mujumdar M, Sanjay J, Goswami BN (2016) Deciphering the desiccation trend of the South Asian monsoon hydroclimate in a warming world. *Clim Dyn* 47:1007–1027. <https://doi.org/10.1007/s00382-015-2886-5>
- Kumar KK, Rajagopalan B, Cane MA (1999) On the Weakening Relationship Between the Indian Monsoon and ENSO, 284(June), 2156–2160
- Lamb HH (1965) The early medieval warm epoch and its sequel. *Palaeogeogr Palaeoclimatol* 1:13–37
- Lehmann J, Coumou D, Frieler K (2015) Increased record-breaking precipitation events under global warming. *Clim Change*. <https://doi.org/10.1007/s10584-015-1434-y>
- Lewis SC, Legrande AN (2015) Stability of ENSO and its tropical Pacific teleconnections over the Last Millennium. *Climate of the Past* 11(10):1347–1360. <https://doi.org/10.5194/cp-11-1347-2015>
- Liu F et al. (2016) Global monsoon precipitation responses to large volcanic eruptions. *Sci Rep*. <https://doi.org/10.1038/srep24331>
- Mann ME, Cane MA, Zebiak SE, Clement A (2005) Volcanic and solar forcing of the tropical Pacific over the past 1000 years. *J Clim* 18:447–456
- Mann M et al (2009) Global signatures and dynamical origins of the Little Ice Age and Medieval Climate Anomaly. *Science* 326:1256–1260
- Mann ME, Zhang Z, Rutherford S, Bradley RS, Hughes MK, Shindell D, Caspar A. Global Signatures and Dynamical Origins of the Little Ice Age and Medieval Climate Anomaly *Science* 27 Nov 2009: Vol. 326, Issue 5957, pp. 1256–1260 <https://doi.org/10.1126/science.1177303>
- Min YM (2008) A Probabilistic Multimodel Ensemble Approach to Seasonal Prediction, 812–828. <https://doi.org/10.1175/2008WAF2222140.1>
- Nakamura A, Yokoyama Y, Maemoku H, Yagi H, Okamura M, Matsuoka H, Miyake N, Osada T, Adhikari DP, Dangol V (2015) Weak monsoon event at 4.2 ka recorded in sediment from

- Lake Rara, Himalayas. *Quat*. <https://doi.org/10.1016/j.quaint.2015.05.053>
- Neff U, Burns SJ, Mangini A, Mudelsee M, Fleitmann D, Matter A (2001) Strong coherence between solar variability and the monsoon in Oman between 9 and 6 kyr ago. *Nature* 411:290–293
- PAGES 2 k Consortium (2013) Continental-scale temperature variability during the last two millennia. *Nature Geosci* 6:339–346
- Pant GB, Rupa Kumar K (1997) *Climates of South Asia*. J. Wiley and Sons, 317 pp
- Ponton C, Giosan L, Eglinton TI, Fuller DQ, Johnson JE, Kumar P, Collett TS (2012) Holocene aridification of India. *Geophys Res Lett* 39:L03704
- Power S, Delage F, Chung C, Kociuba G, Keay K (2013) Robust twenty-first-century projections of El Niño and related precipitation variability. *Nature* 502:541–545. <https://doi.org/10.1038/nature12580>
- Prasad S, Enzel Y (2006) Holocene paleoclimates of India. *Quat Res* 66(3):442–453
- Prasad S, Anoop A, Riedel N, Sarkar S, Menzel P, Basavaiah N, Krishnan R, Fuller D, Plessen B, Gaye B, Röhl, U, Wilkes, H, Sachse D, Sawant R, Wiesner B, Stebich M (2014) Prolonged monsoon droughts and links to Indo-Pacific warm pool: a Holocene record from Lonar Lake, Central India. *Earth Planet Sci Lett* 391:171–182
- Rajeevan M, Bhate J, Kale JD, Lal B (2006) High resolution daily gridded rainfall data for the Indian region?: Analysis of break and active monsoon spells, 91(3)
- Ramesh R, Tiwari M, Chakraborty S, Managave SR, Yadava MG, Sinha DK (2010) Retrieval of south asian monsoon variation during the holocene from natural climate archives. *Curr Sci* 99(12):1770–1786
- Revadekar JV, Kothawale DR, Patwardhan SK, Pant GB, Kumar KR (2012) Extremes over India, 1133–1155. <https://doi.org/10.1007/s11069-011-9895-4>
- Roxy MK, Ritika K, Terray P, Murtugudde R, Ashok K, BN Gowswami (2015) Drying of Indian subcontinent by rapid Indian Ocean warming and a weakening land-sea thermal gradient—*Nature communications*, 2015
- Sano M, Ramesh R, Sheshshayee M, Sukumar R (2011) Increasing aridity over the past 223 years in the Nepal Himalaya inferred from a tree-ring  $\delta^{18}\text{O}$  chronology. *The Holocene*, 1–9
- Sarkar A, Ramesh R, Somayajulu BLK, Agnihotri R, Jull AJT, Burr OS (2000) High resolution Holocene monsoon record from the eastern Arabian Sea. *Earth Planet Sci Lett* 177(3–4):209–218. [https://doi.org/10.1016/S0012-821X\(00\)00053-4](https://doi.org/10.1016/S0012-821X(00)00053-4)
- Schmidt MWI, Co-authors. Persistence of soil organic matter as an ecosystem property. *Nature*. 2011/10/06/print, 478, Nature Publishing Group, <https://doi.org/10.1038/nature10386>
- Schmidt GA, Jungclaus JH, Ammann CM, Bard E, Braconnot P, Crowley TJ, Delaygue G, Joos F, Krivova NA, Muscheler R, Otto-Bliessner BL, Pongratz J, Shindell DT, Solanki SK, Steinhilber F, Vieira LEA (2012) Climate forcing reconstructions for use in PMIP simulations of the Last Millennium (v1.1). *Geosci Model Dev* 5:185–191. <https://doi.org/10.5194/gmd-5-185-2012>
- Sikka DR (1980) Some aspects of the large scale fluctuations of summer monsoon rainfall over India in relation to fluctuations in the planetary and regional scale circulation parameters. *Proc. Ind. Acad. Sci.*, 89, 179–195
- Sinha A, Cannariato KG, Stott LD, Cheng H, Edwards RL, Yadava MG, Ramesh R, Singh IB (2007) A 900-year (600 to 1500 AD) record of the Indian summer monsoon precipitation from the core-monsoon zone of India. *Geophys. Res. Lett.* 34
- Sinha A, Gayatri Kathayat H, Cheng, Sebastian FM, Breitenbach M, Berkelhammer M, Mudelsee J (2015) Trends and oscillations in the Indian summer monsoon rainfall over the last two millennia. *Nat Commun*. <https://doi.org/10.1038/ncomms7309>
- Staubwasser M, Sirocko F, Grootes PM, Segl M (2003) Climate change at the 4.2 ka BP termination of the Indus valley civilization and Holocene south Asian monsoon variability. *Geophys Res Lett* 30:1425. <https://doi.org/10.1029/2002GL016822>
- Stocker TF, Qin D, Plattner G-K, Alexander LV, Allen SK, Bindoff NL, Bréon F-M, Church JA, Cubasch U, Emori S, Forster P, Friedlingstein P, N. Gillett JM, Gregory DL, Hartmann E, Jansen B, Kirtman R, Knutti K, Krishna Kumar P, Lemke J, Marotzke V, Masson-Delmotte GA, Meehl II, Mokhov S, Piao V, Ramaswamy D, Randall M, Rhein M, Rojas C, Sabine D, Shindell LD, Talley DG, Vaughan, Xie S-P (2013) Technical Summary. *Climate Change 2013: The Physical Science Basis. Contribution of Working Group I to the Fifth Assessment Report of the Intergovernmental Panel on Climate Change* [Stocker, Qin TF, D, Plattner G-K, Tignor M, Allen SK, Boschung J, Nauels A, Xia Y, Bex V, Midgley PM (eds.)]. Cambridge University Press, Cambridge, pp 33–115. [https://doi.org/10.1017/CBO9781107415324\\_4005](https://doi.org/10.1017/CBO9781107415324_4005)
- Taylor KE, Stouffer RJ, Meehl GA (2012) An overview of CMIP5 and the experiment design. *B Am Meteorol Soc* 93:485–498. <https://doi.org/10.1175/BAMS-D-11-00094.1>
- Thamban M, Kawahata H, Rao VP (2007) Indian Summer Monsoon Variability during the Holocene as Recorded in Sediments of the Arabian Sea: Timing and Implications. *J Oceanogr* 63(6):1009–1020 2007
- Titchner HA, Rayner NA (2014) The Met Office Hadley Centre sea ice and sea surface temperature data set, version 2: 1. Sea ice concentrations. *J Geophys Res Atmos* 119:2864–2889. <https://doi.org/10.1002/2013JD020316>
- Tiwari M, Ramesh R, Somayajulu B, Jull A, Burr G (2005) Solar control of southwest monsoon on centennial timescales. *Curr Sci* 89:1583–1588
- Trenberth KE, Caron JM, Stepaniak DP, Worley S (2002) Evolution of El Niño–Southern Oscillation and global atmospheric surface temperatures. *J Geophys Res*. <https://doi.org/10.1029/2000JD000298>
- Vecchi GA, Soden BJ, Wittenberg AT, Held IM, Leetmaa A, Harrison MJ (2006) Weakening of tropical Pacific atmospheric circulation due to anthropogenic forcing 441:73–76. <https://doi.org/10.1038/nature04744>
- Wanner H, Beer J, Buetikofer J, Crowley TJ, Cubasch U, Flueckiger J, Goosse H, Grosjean M, Joos F, Kaplan JO (2008) Mid-to Late Holocene climate change: an overview. *Quat Sci Rev* 27:1791–1828
- Wittenberg AT (2009) Are historical records sufficient to constrain ENSO simulations? *Geophys Res Lett* 36:L12702. <https://doi.org/10.1029/2009GL038710>
- Xie P, Arkin PA (1997) Global precipitation: a 17-year monthly analysis based on gauge observations, satellite estimates, and numerical model outputs. *Bull Amer Meteorol Soc* 78:2539–2558
- Yadava MG, Ramesh RR (2005) Monsoon reconstruction from radiocarbon dated tropical speleothems. *The Holocene* 15:48–59